MJFAS
Malaysian Journal of Fundamental and Applied Sciences

Zahidi *et al.* | Malaysian Journal of Fundamental and Applied Sciences, Vol. 22 (2026) 454–465

RESEARCH ARTICLE

Fabrication of Plasmonic Pt/Au-coated Micro-Peanut Fiber Probe Using Heat-and-Pull Technique for Enhanced Light Coupling Efficiency

Nurul Auni Afifah Ahmad Zahidi[a], Wan Maisarah Mukhtar[a*], Wan Nursyafiqah Wan Harun[a], Razman Mohd Halim[b], Affa Rozana Abdul Rashid[a], Syahida Suhaimi[a]

[a]Faculty of Science and Technology, Universiti Sains Islam Malaysia (USIM), Bandar Baru Nilai, 71800 Nilai, Negeri Sembilan, Malaysia; [b]National Metrology Institute of Malaysia (NMIM), Bandar Baru Salak Tinggi, Malaysia

Abstract The aim of this study is to fabricate a micro-lens for enhanced light coupling efficiency based on plasmonic effect by modifying the structure of fiber end into the micro-peanut shape using a low-cost heat-and-pull technique, coated with gold nanoparticles and platinum thin film. The fabrication process involves the usage of a Z2C core alignment fusion splicer by varying few important parameters including arc power, arc time, fiber pulling and fiber pulling length. During tapering, the fiber optics experienced structural modification from bi-tapered structure to the formation of micro-peanut fiber probe. Platinum thin film and gold nanoparticles in a form of nanospheres and nanorods are deposited onto the fiber probe to transport electromagnetic energy in micro and nanoscale with high efficiency. The transition process for forming the micro-peanut structure begins with the fabrication of a bi-tapered microfiber. This bi-tapered structure consists of two tapered regions, with tapered lengths ranging from 0.109 to 0.127 mm and taper angles between 53.68° and 65.10°. Subsequently, the micro-peanut probe develops a distinct peanut-like geometry, characterized by ellipsoidal sections with tip radii ranging from 0.051 to 0.080 mm. Greater nano-focusing assisted by surface plasmon polariton with maximum coupling efficiency up to 95.40% is successfully achieved by utilizing gold nanorods with a platinum-coated micro-peanut probe. The LSPR effect clearly enhances light–matter interactions, maximizing nano-focusing for light coupling and enabling optical trapping applications. This study presents a highly efficient light-coupling approach with broad potential applications, ranging from biosensing to biomedical fields.

Keywords: Light coupling, heat-and-pull, micro-peanut, ball-lens fiber probe, plasmonic.

***For correspondence:**
wmaisarah@usim.edu.my

Received: 3 Nov. 2025
Accepted: 29 Jan. 2026

Introduction

A major hurdle in the field of integrated photonics is the efficient coupling of light from a standard optical fiber to devices. These issues affect significant impacts in signal losses in various applications including digital computing and quantum optics [1, 2]. Over the past years, researchers have proposed various approaches to optimize the coupling efficiency of fiber probe such as by designing the photonic lanterns, fabricating the fiber tapered structures and introducing the fiber bundles which are costly [3-6]. In optical coherence tomography (OCT), few technologies have been introduced including the utilization of gradient refractive index (GRIN) which allows for compact, lightweight designs that can achieve optical effects like focusing or collimating light [7-9]. In civil engineering, deployment of focusing system is crucial for the measurement of floor space index (FSI) to enhance coupling efficiency so that the optical probe successfully able to target distance. The main challenge in developing an excellent focusing optical system is to ensure maximum coupling efficiency when target distance changes. Therefore, it is of great importance to study how coupling efficiency varies with distance, probe's structure and its numerical aperture (NA) [10-13]. Note that a small deflection may lead to a significant decrease in coupling efficiency.

One of the hiccups of probing light-matter interaction in nanoscale level is the efficient light delivery from input to output. In optical spectroscopy, it is authoritative that light be confined to a small space in the order of nanoscales. Surface plasmon resonance (SPR) is a phenomenon where light is interacted with noble metal such as gold, platinum and silver resulting the generation of surface plasmon polaritons at nanoscale [14-16]. The deployment of noble metal nanoparticles like nanorods, nanospheres and nanowires resulted the excitation of localized surface plasmons (LSPs) [17]. LSPs are oscillations of charge density that occur within metal nanoparticles. The ability of LSPs to concentrate electromagnetic fields in the presence of the nanoparticles enables the enhancement of the interaction between light and matter, resulting to increased sensitivity and selectivity in detection and imaging techniques [18-20]. Recently, studies have shown that optical fiber-incorporated metal-coated plasmonic probes, such as gold and platinum can be a platform for transporting electromagnetic energy in nanoscale with high efficiency [21-23]. Efficient coupling of linearly polarized excitation to radial plasmons is highly desirable for various significance of applications ranging from biosensing to near-field spectroscopy.

The aim of this study is to fabricate a fiber probe micro-lens based on plasmonic effect by modifying the structure of fiber end into the micro-peanut shape using a low-cost heat-and-pull technique. The spherical end shape of the proposed probe enhances the coupling efficiency by collimating light to minimize mode mismatch. The LSPR effect is incorporated by depositing platinum thin film and gold nanoparticles (gold nanorods and gold nanospheres) on the surface of micro-probe in which enable the enhancement of the light interaction leading to maximize the nano-focusing for the future application in optical trapping. We believe that the output of this study offers a highly efficient light coupling approach with broaden applications including biomedical fields.

Materials and Methods

Fabrication of Micro-peanut Probe using Heat-and-pull Technique

The fabrication of micro-peanut probe was performed via heat-and-pull technique by using a standard optical communication fusion splicer (Brand: Z2C Core Alignment Fusion Splicer Sumitomo Electric). First, a standard single mode fiber (SMF28) with core diameter of 9/125 μm was placed on the V-groove holder inside the fusion splicer. To ensure symmetrical shapes for both fabricated probe later, the centre part of fiber optic was positioned directly opposite to the electrodes as illustrated in Figure 1(a). Next, the heat-and-pull technique was performed by controlled the important parameters included arc time ranging from 1.0 to 1.6 seconds, arc power from 60 to 91 steps, prefuse time of 0.8 seconds, a constant of fiber pulling start of 4 seconds, fiber pulling lengths between 45 mm and 50 mm, and fiber pulling speeds between 400 and 500 pulses per second (pps). Combination of heating by electric arc discharge and pulling process resulted the formation of bi-tapered fiber as shown in Figure 1(b). Once the fiber break, both sides of the tapered fiber formed hemispherical shape, namely the micro-peanut structure due to the heating effect produced by electric arc discharge (Figure 1(c)). In this study, five samples of micro-peanut probes with various radii were prepared. A digital microscope (Brand: Dino-Lite) was used to analyze the geometrical properties of the bi-tapered fiber and micro-peanut probe. Table 1 shows the control parameters for the probe's fabrication.

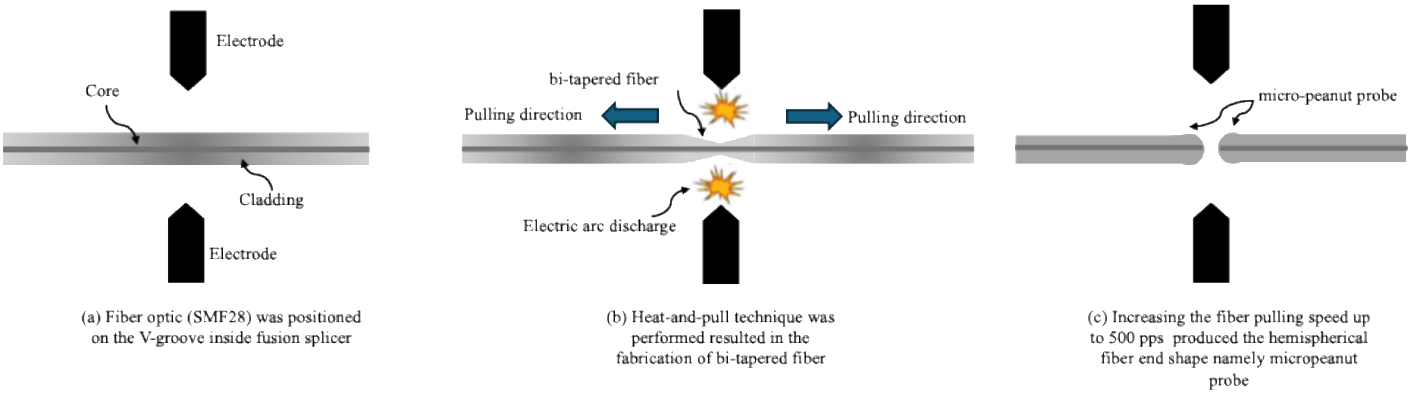

(a) Fiber optic (SMF28) was positioned on the V-groove inside fusion splicer

(b) Heat-and-pull technique was performed resulted in the fabrication of bi-tapered fiber

(c) Increasing the fiber pulling speed up to 500 pps produced the hemispherical fiber end shape namely micropeanut probe

Figure 1. Schematic diagram for fabrication process of micro-peanut probe using heat-and-pull technique

Table 1. Control parameters to fabricate fiber probe using heat-and-pull technique

Parameters	Values
Arc time	1.0 to 1.6 seconds
Arc power	60 to 91 steps
Prefuse time	0.8 seconds
Fiber pulling start	4 seconds
Fiber pulling length	45 mm to 50 mm
Fiber pulling speed	400 to 500 pps

Deposition of Pt and Au Nanoparticles on Micro-peanut Probe

To study the effect of SPR on the optical coupling performance of the fabricated probe, two types of noble metal layers were deposited on the probe's surface as depicted in Table 2. Platinum thin film was deposited onto the substrate by using a sputtering technique (Brand: JEC-3000FC Auto fine Sputter Coater). The probes were placed on a fiber holder to secure the probes during the sputtering process. The parameters such as deposition time and power setting were maintained at 15 seconds and 10 mA respectively. The deposition of gold nanoparticles with two different nanostructures namely gold nanorods and gold nanospheres were performed by soaking the probes into those liquid solution for four hours before left them dried for eight hours at room temperature. The optical properties of Pt, AuNR and AuNP were characterized by using UV-Vis spectroscopy.

Table 2. Samples with various configuration

Sample	Configuration
1	Pt monolayer
2	AuNP monolayer
3	AuNR monolayer
4	Pt/AuNP bilayer
5	Pt/AuNR bilayer

Analysis of Light Coupling Efficiency

The fabricated micro-peanut probes were connected to the optical power meter (OPM) and optical spectrum analyzer (OSA). The position of probe was properly aligned with the multi-mode fiber as illustrated in Figure 2. Multi-mode fiber which connected to the optical light source (OLS) acted as transmitter. Note that the deployment of MMF with higher numerical aperture (NA) than single mode fiber (SMF) allowing better light coupling from the transmitter [24]. A light coupling was performed by positioning the flat-ended cleaved multimode fiber parallel with the probe. The distance between micro-peanut probe and multimode fiber was varied from 1 mm to 5 mm with an increment of 1 mm for each reading. The light coupling efficiency was calculated by using Equation [1]:

$$\text{Coupling efficiency} = P_{out}/P_{in} \quad (1)$$

where P_{out} and P_{in} are the measured optical power values from the power meter in watts (W). The ratio of optical power P_{out} to P_{in} provides the coupling efficiency which serves as a measure of the effectiveness of optical power transfer between the probes. Greater value of coupling efficiency ($\cong$ 1.0 a.u) exhibits excellent light transfer from transmitter to the receiver. Taking into account key factors such as Fresnel loss and air turbulence, the influence of wavelength on light coupling efficiency was systematically investigated at 1310 nm and 1550 nm, as these wavelengths exhibit minimal attenuation in both free-space propagation and fiber-optic transmission [25]. These procedures were repeated for Pt-coated micro-peanut probe and Pt/Au coated micropeanut probe configurations with various probe's diameters.

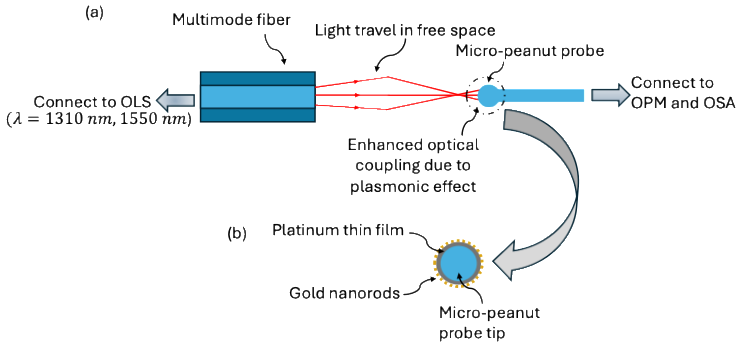

Figure 2. Experimental setup for light coupling (a) multimode fiber acted as transmitter and micro-peanut probe as light coupler (b) the inset shows the micro-peanut probe tip coated with platinum and gold nanorods to generate localized surface plasmon resonance

Results and Discussion

Structural Analysis of bi-tapered Fiber and Micro-peanut Probe Fabricated by Heat-pull Technique

Figure 3 displays the microscope images along with measurements for each bi-tapered fiber samples. With both electrodes positioned at the center of the optical fiber and identical pulling distance and speed applied, the two sides of the bi-tapered region exhibited comparable taper lengths and taper angles. The range of tapered length was obtained within 0.109 mm and 0.127 mm with percentage of decrement about 14.17% as the applied arc power increased from 50 steps to 0.76 steps. Meanwhile, the tapered angles also shows the same pattern in which the values decreased up to 17.54% in the range between 53.68° and 65.10° as depicted in Figure 4. By focusing suitable value for each parameter, we successfully optimized the procedure to fabricate micro-peanut fiber structure.

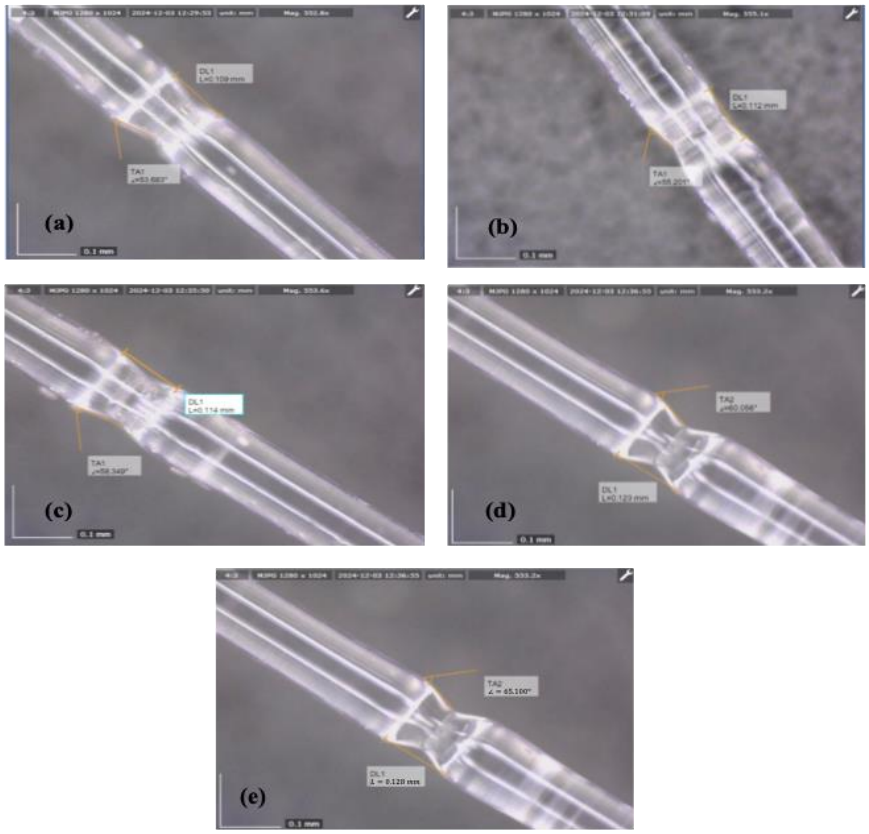

Figure 3. Image of the bi-tapered fibers captured under a digital microscope with tapered length value of 0.109 mm to 0.127 mm and angle between 53.68° to 65.10° (a) bi-tapered 1(*l*=0.127 mm, θ=65.10°) (b) bi-tapered 2 (*l*=0.123 mm, θ=60.06°) (c) bi-tapered 3 (*l*=0.114 mm, θ=58.35°) (d) bi-tapered 4 (*l*=0.112 mm, θ=55.20°) (e) bi-tapered 5 (*l*=0.109 mm, θ=53.68°)

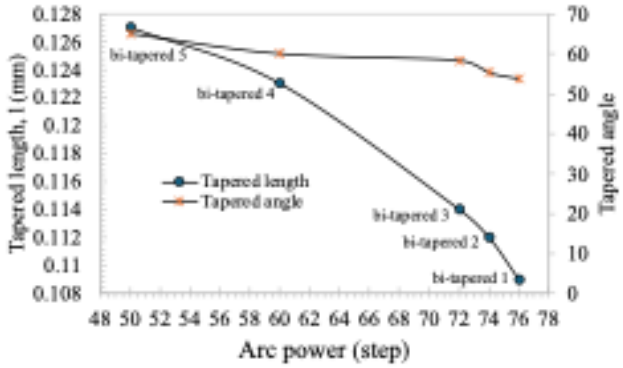

Figure 4. Increasing arc power, *P* resulted smaller tapered angle, θ and smaller tapered length, *l* of fiber

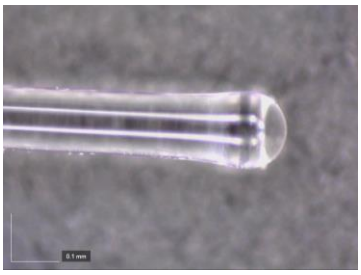

Figure 5. Micro-peanut probe represented by hemispherical structure at the fiber end fabricated by heat-and-pull technique

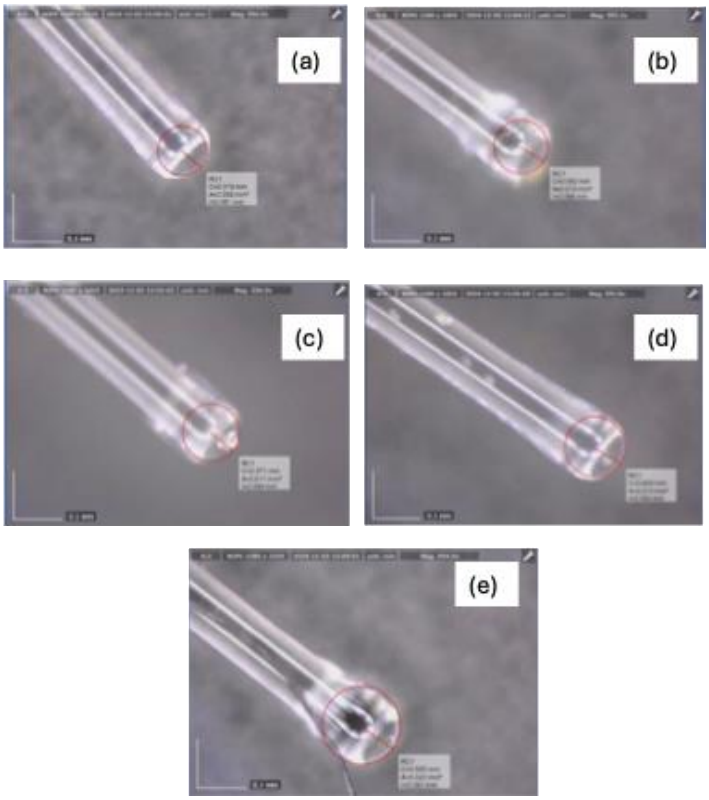

Figure 6. Image of the micro-peanut probe captured under a digital microscope with tip radius, *r* between 0.051 mm to 0.080 mm (a) Probe 1 (*r* = 0.051 mm) (b) Probe 2 (*r* = 0.056 mm) (c) Probe 3 (*r* = 0.059 mm) (d) Probe 4 (*r* = 0.064 mm) (e) Probe 5 (*r* = 0.080 mm)

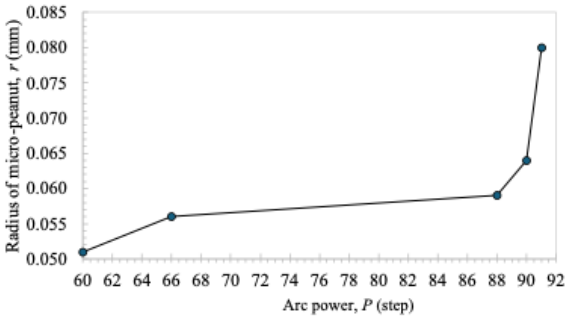

Figure 7. Radius of micro-peanut probe, *r* increased with the increment of arc power, *P*

Figure 5 depicts the image of the micro-peanut probe represented by hemispherical shape at the tip part as the arc power reached 60 steps by using heat-and-pull technique. Its hemispherical shape plays an important function for efficient light coupling due to its low divergence and good mode matching [26]. To fabricate the hemispherical structure with numerous radii as shown in Figure 6(a)-(e), the arc power was varied from 60 steps to 91 steps while maintained the pulling time and pulling speed at 4 s and 500 pps respectively; resulting the radii of micro-peanut probes ranging from 0.051 mm until 0.080 mm. The micro-peanut's radii increased up to 56.86% with the increment of arc power indicated the crucial role of electrical parameter in producing the desired structure of probe (Figure 7). It should be noted that the optimized micro-peanut structure was determined based on the smallest radius, as it provides enhanced nano-focusing capability. In this study, the best radius of micro-peanut structure was found to be 0.051 mm.

Optical Characterization of Platinum Thin Film and Gold Nanoparticles

UV–Vis analysis was conducted to confirm the types of metals used in this study, namely Pt, AuNR, and AuNS. The characterization was based on the position and intensity of the surface plasmon resonance peaks, which are sensitive to particle size and shape [27]. Figure 8(a) shows the UV-Vis spectrum of platinum thin film coated on glass slide using sputtering technique. The absence of a sharp absorbance peak instead of broad absorption in the visible range confirms that the optical response of the Pt thin film is governed by interband transitions rather than plasmonic resonance, with dominant absorption occurring in the ultraviolet region [28]. However, in recent years, Pt has gained attention as a promising alternative to gold for surface plasmon resonance (SPR) excitation due to its chemical stability and broadband optical response [29]. Figure 8(b) exhibits the UV-Vis analysis of gold nanorods (AuNR) and gold nanospheres (AuNS) coated on the glass substrate. The presence of absorbance peak around 520-530 nm exhibits the optical properties of AuNS due to the transverse peak arises from the oscillation of electron.

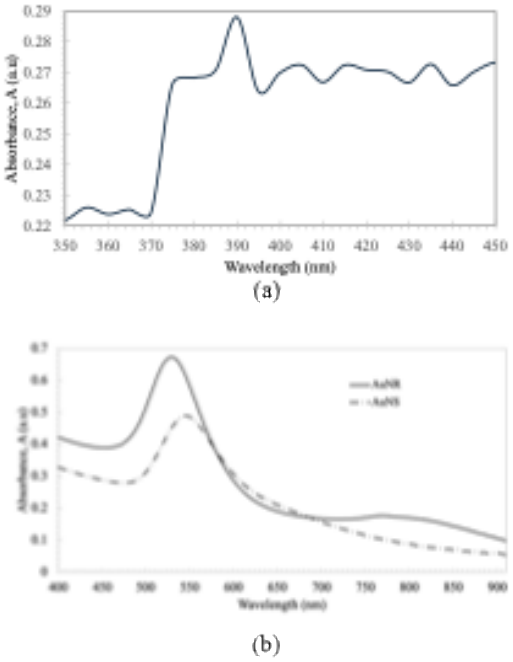

Figure 8. UV-Vis spectra (a) platinum with 30nm thickness (b) gold nanorods (AuNR) and gold nanospheres (AuNS)

AuNR exhibit two absorption peaks due to surface plasmon resonance a transverse peak around 520-530 nm and a longitudinal peak that is sensitive to the aspect ratio and can range from the visible to the near-infrared (NIR) region (750 – 800 nm). Note that the longitudinal peak results from the oscillation along the longer axis. The deployment of these two types of noble metal successfully generated SPR signal that will be used to enhance the optical coupling effect.

Effect of bi-tapered Structures of Microfibers to the Optical Power Level

Figure 9(a) provides insight into the optical behavior of the bi-tapered fiber with various tapered length and diameter characterized using the optical spectrum analyzer (OSA). The peaks mostly fell between -53 dB and -33 dB which were labeled as bi-tapered 1, bi-tapered 2, bi-tapered 3, bi-tapered 4 and bi-tapered 5. Bi-tapered 2 consistently shows the highest peak intensity, while bi-tapered 1 tends to demonstrate slightly lower intensities. It can be concluded that the 1310 nm spectrum exhibits consistency in peak intensity and wavelength spacing, indicating that this wavelength is less sensitive to external perturbations. This stability makes 1310 nm suitable for applications that focus on reliability over sensitivity. In contrary, the 1550 nm uncoated bi-tapered microfibers showed a significantly shorter number of peaks occurring at shorter time intervals compared to the 1310 nm graph as illustrated in Figure 9(b). Peaks appeared at regular intervals, such as 1552 nm, 1553 nm, and 1554 nm. Among all sample, bi-tapered 2 showed the highest intensity that reached intensity levels near -20 dB, while bi-tapered 4 showed lower intensity, which ranged from -35 dB to -40 dB. The intensity levels for 1550 nm exhibited the same ranges as 1310 nm which ranged from -20 dB to -55 dB, but with greater variability. The wavelength range started from 1550 nm to 1562 nm, which was wider than the observed range at 1310 nm. Moreover, the slight difference between the 1550 nm spectral peak reflected a greater refractive index sensitivity. This makes this wavelength more responsive to the changes in the environment or other parameters variations. Comparing these two spectra, the 1550 nm spectrum showed greater sensitivity due to the variation in peak intensity and higher number of peaks. Consequently, the 1550 nm wavelength is particularly suitable for applications requiring high-precision detection, such as optical coupling and optical trapping, due to its enhanced sensitivity. In contrast, the 1310 nm spectrum exhibits greater stability, with a consistent peak intensity across the tested parameter set. This stability makes 1310 nm ideal for applications where environmental influences must be minimized, such as in stable optical systems with lower sensitivity requirements.

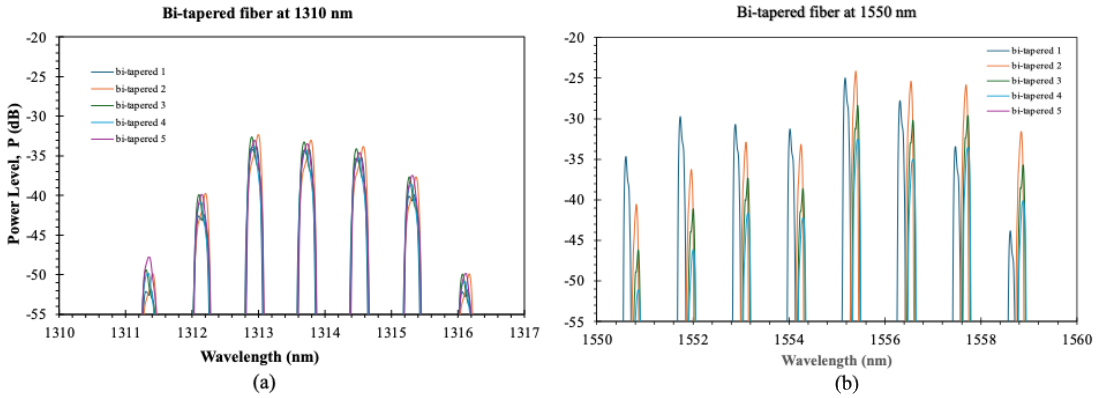

Figure 9. Effect of bi-tapered structures to the optical power level using OSA (a) λ=1310 nm (b) λ=1550 nm

Analysis of Light Coupling Efficiency with Various Coupling Distance using Monolayer Noble Metal Coated Micro-peanut Probe

Figure 10(a) shows variation optical power ratio (P_{output}/P_{input}) as gold nanospheres (AuNS) coated micro-peanut probes with different radii were connected to the light source with wavelength, λ=1310 nm. All micro-peanut probes experienced consistent coupling efficiency of 1.000 a.u in which proves the maximum coupling efficiency at shortest distance. At the coupling distance increased, the coupling efficiency of probe 1 decreased compatibly, reaching 0.878 a.u at distance of 5 mm. This indicated poor stability of power as the distance increased. Probe 2 demonstrated better performance than probe 1 but still occurred a drop in coupling efficiency about 5.92 % to 0.930 a.u at 5 mm. Next, probe 3 showed an increment in efficiency starting from distance of 3 mm onward that exhibits peak at 1.052 a.u at 5 mm which represented an improvement at longer distances. Probe 4 performed well at shorter distances such as 1 mm to 3 mm but began to decline as the distance increases. Lastly, probe 5 was the ideal probe with the coupling efficiency increasing at longer distances which reaching 1.041 a.u at 5 mm. Probe 5 maintained a stable increase of power ratio across all distances. This was due to larger coupling radius of probe 5 which was 0.080 mm that allowing the probe to capture more diverging laser beams that emitted from the light source in free space conditions that leading to better coupling efficiency especially at longer distances. It is observed that the size of coupling lens plays an important role in maximizing the coupling efficiency. The effect of multimode beams on the coupling becomes apparent with the further increase in probe's radii [30]. As wavelength increased to λ=1550 nm (Figure 10(b)), all probes exhibited similar power ratio value of 1.000 a.u with a slight increase in the coupling efficiency up to 1.038 a.u at 3 mm but started dropped sharply about 10.50 % to 0.929 a.u at 5 mm, indicating instability in coupling efficiency at longer distances. In contrary, probe 2 showed consistent performance with small fluctuations in the power ratio value as the distance increased. Nonetheless, the coupling efficiency dropped to 0.951 a.u at 5 mm reflecting a better stability compared to probe 1. Probe 3 experienced the rise in the light coupling where it peaked at 1.034 a.u at 2 mm then decreased about 9.86 % to 0.932 a.u at 5 mm. However, probe 4 showed a constant decrease in coupling efficiency as the distance increased reaching a lowest value of 0.955 a.u at 5 mm proving moderate coupling performance over longer distances. Probe 5 maintained the best overall stability and coupling efficiency with power value ratio of 0.961 a.u at 5 mm. Note that, the apparent increase in output power ($P_{out}>P_{in}$) resulting in the value of coupling efficiency greater than 1.000 a.u, does not indicate optical amplification; rather, it arises from enhanced light collection and mode confinement enabled by localized surface plasmon resonance at the metal-coated fiber probe. The plasmonic structure improves spatial mode matching between the incident free-space beam and the guided fiber mode, allowing a larger fraction of the incident optical power to be efficiently coupled into the fiber [31].

Figure 11 illustrates the effect of Pt-coated micro-peanut probe with various radii to the optical power ratio as the coupling distance increased from 1 mm to 5 mm. The performance of the micro-peanut probe at wavelength of 1310 nm demonstrates efficient coupling behaviour across varying distances (Figure 11(a)). At a starting distance of 1 mm, the coupling efficiency was approximately 1.100 a.u, indicating excellent coupling efficiency. As the distance increased, the power ratio gradually declined up to 27.27 %, reaching a value of around 0.800 a.u at 5 mm. This consistent decrease in power ratio reflects the expected attenuation of light with increasing distance due to mode mismatch or coupling loss. The results across all five probes showed minimal variation, highlighting the reproducibility and reliability of the fabrication process. Overall, the micro-peanut probe maintained a high level of coupling efficiency at

1310 nm, making it well-suited for applications where coupling performance at shorter to moderate distances is critical.

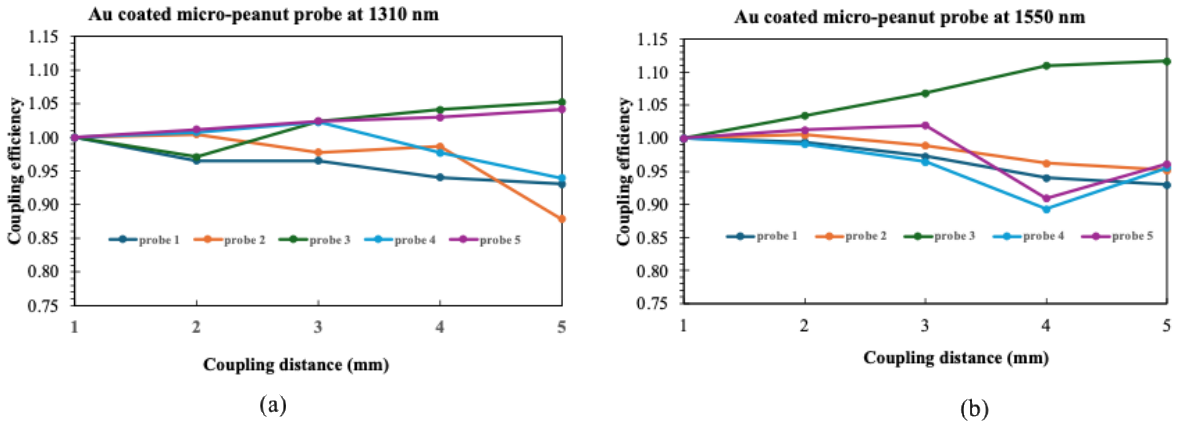

Figure 10. Effect of AuNS coated micro-peanut probe with various radii to the coupling efficiency as distance increased (a) λ=1310 nm (b) λ=1550 nm

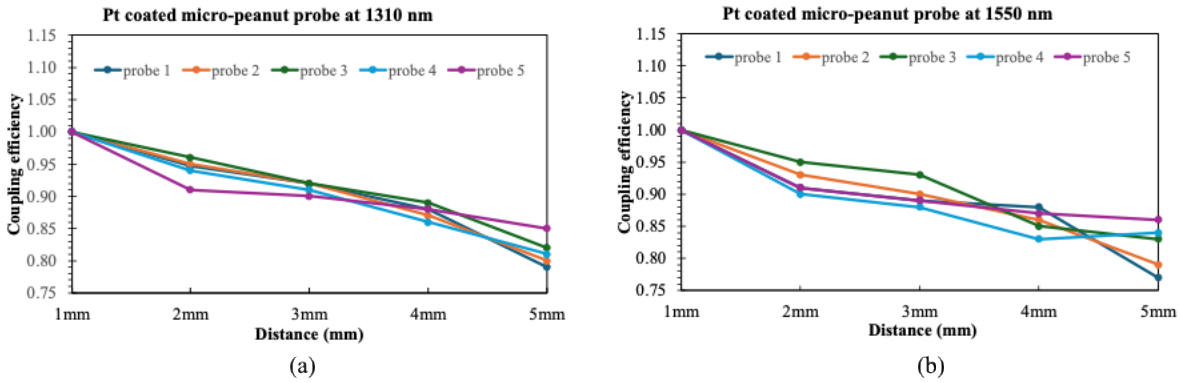

Figure 11. Effect of Pt coated micro-peanut probe with various radii to the coupling efficiency as distance increased (a) λ=1310 nm (b) λ=1550 nm

The micro-peanut probe also exhibited efficient coupling at a higher wavelength of 1550 nm as shown in Figure 11(b). At the shortest distance of 1 mm, the coupling efficiency began at approximately 1.050 a.u, slightly lower about 4.76% than the value observed at 1310 nm. As the distance increased, the coupling efficiency declined steadily, reaching a value of around 0.750 a.u at 5 mm. The decrease in power ratio at 1550 nm was slightly more pronounced compared to 1310 nm, which could be attributed to the wavelength-dependent characteristics of the probe. Despite the slight reduction in coupling efficiency, the consistent trends observed across all five probes underscored the reliability of the micro-peanut design. This probe is particularly suited for applications requiring uniform performance across multiple probes, even though it may be slightly less efficient at longer distances at this wavelength.

Analysis of Light Coupling Efficiency with Various Coupling Distance using Different Bilayer Noble Metal Nanostructures Coated Micro-peanut Probe

Figure 12(a) shows the analysis of power ratio between incident wavelength, λ=1310 nm and λ=1550 nm using bilayer Pt/AuNS-coated micro-peanut probe. Obviously, both 1310 nm and 1550 nm wavelengths exhibited a decrease in power output ratio as the distance increased from 1 mm to 5 mm. One factor contributing to power loss was air turbulence, which primarily occurs in free-space optical systems [25]. It was observed that at 1310 nm, the coupling efficiency dropped from 1.0 a.u at 1 mm distance to 0.954 a.u at 5 mm with 4.55 % reduction. Meanwhile, at 1550 nm the coupling efficiency decreased from 1.0 a.u to 0.917 a.u with reduction of 8.29 %. This indicates that the coupling efficiency at 1310 nm decreased more gradually retaining higher values at each distance. This situation explained

better retention of light coupling over distance compared to 1550 nm that showed a steeper drop meaning more light was lost over the increasing distance during the light coupling. Fresnel loss was also considered, resulting in power loss at the air–micro-peanut probe interface due to the difference in their refractive indices [32].

For Pt/AuNR-coated micro-peanut probes (Figure 12(b)), the coupling efficiency decreased from 1.0 a.u to 0.978 a.u as the distance increased resulting in a 2.42 % reduction at 1310 nm wavelength. At 1550 nm, the coupling efficiency showed a greater reduction of 4.76% as the value decreased from 1.0 a.u to 0.952 a.u. This indicates that 1310 nm provides better compatibility with the optical properties of the Pt/AuNR-coated micro-peanut probes, leading to more efficient power transmission for light coupling process. Apparently, at both 1310 nm and 1550 nm, the Pt/AuNR-coated micro-peanut probes offers a better coupling efficiency compared to Pt/AuNS even though both show a steep decline in power output ratio. Thus, AuNR was more effective choice for maintaining efficient light coupling over longer distances. The core waveguide mode guided in the transmitter can be coupled to plasmons on the surface of bilayer Pt/AuNR coated on the micro-peanut end fiber. The coupled plasmonic mode then propagates to the spherical apex where it is localized and strongly focused, resulting immense longitudinal field enhancement [33]. Obviously, the surface plasmon resonance effect could enhance the light absorption of materials. By concluding the plasmonic-enhanced light coupling efficiency, we show that the performance of Pt/AuNR-coated micro-peanut probe has been significantly improved due to the addition of plasmonic structures.

In comparison with a conventional uncoated peanut-fiber probe, an LSPR-based micro-peanut probe offers enhanced light coupling through localized electromagnetic field amplification induced by noble-metal nanostructures integrated at the lens surface [34, 35]. While a standard micro-peanut probe improves coupling efficiency primarily through refractive beam shaping to enhance spatial mode matching and alignment tolerance, the incorporation of plasmonic nanostructures enables localized surface plasmon resonance, leading to strong near-field confinement and intensified optical fields at the probe apex [36, 37].

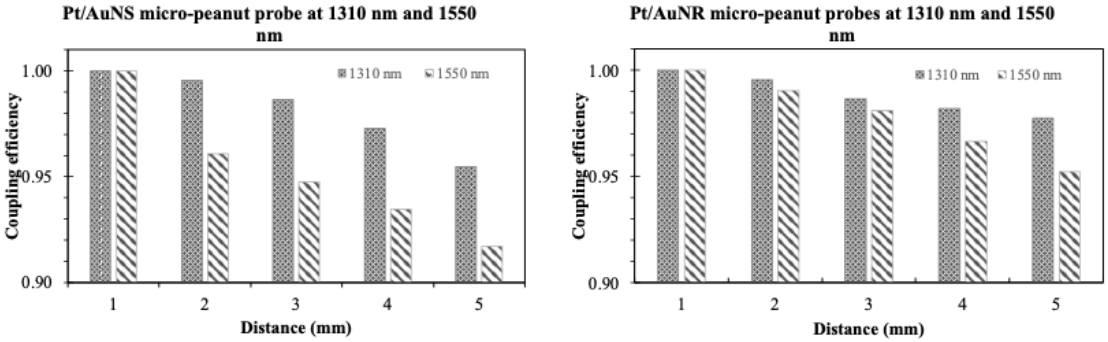

Figure 12. Analysis of coupling efficiency between incident wavelength, λ=1310 nm and λ=1550 nm using different bilayer noble metal coated on micro-peanut probe (a) bilayer gold nanospheres and platinum thin film (Pt/AuNS) (b) bilayer gold nanorods and platinum thin film (Pt/AuNR)

This LSPR-induced field enhancement increases the effective interaction between incident light and guided fiber modes, allowing coupling efficiencies beyond those achievable by geometric optics alone [38]. Compared to tapered or angle-cleaved fiber probes, which are highly sensitive to fabrication accuracy and alignment conditions, the LSPR-based micro-peanut probe retains superior mechanical robustness and repeatability while providing plasmon-assisted coupling enhancement, making it particularly suitable for high-efficiency light coupling in free-space excitation, near-field microscopy, and optical sensing applications [39].

Conclusions

This study introduces a novel micro-probe design, termed the micro-peanut structure, for enhanced light coupling. By leveraging the localized surface plasmon resonance (LSPR) effect through the integration of two types of gold nanostructures and a platinum thin film, the coupling efficiency was significantly

improved. Specifically, replacing Pt/AuNS with Pt/AuNR at an incident wavelength of 1310 nm resulted in an increase in coupling efficiency of up to 48.81%, while deployment at 1550 nm exhibited a similar trend with a 40.57% improvement. Maximum nano-focusing, aided by surface plasmon polaritons, was achieved with the Pt/AuNR-coated micro-peanut probe, reaching a coupling efficiency of 95.40%. These results demonstrate that LSPR enhances light–matter interaction, thereby maximizing nano-focusing for light coupling and optical trapping applications. The plasmonic micro-peanut probe thus represents a promising alternative for high-efficiency light coupling devices, with potential applications spanning from sensing and bio-imaging to broader biomedical fields.

Conflicts of Interest

The authors declare that there is no conflict of interest regarding the publication of this paper.

Acknowledgment

This work is part of a research project under USIM Research Grant (Code no: PPPI/USIM/FST/USIM/110923), supported by the Universiti Sains Islam Malaysia (USIM). The Faculty of Science and Technology (FST), USIM and National Metrology Institute of Malaysia (NMIM) are acknowledged for the research facilities.

References

[1] Iyer, A., Kandel, Y. P., Xu, W., Nichol, J. M., & Renninger, W. H. (2024). Coherent optical coupling to surface acoustic wave devices. *Nature Communications, 15*(1), 3993. https://doi.org/10.1038/s41467-024-3993.

[2] Xu, R., Taheriniya, S., Ovvyan, A. P., Bankwitz, J. R., McRae, L., Jung, E., *et al*. (2023). Hybrid photonic integrated circuits for neuromorphic computing. *Optical Materials Express, 13*(12), 3553–3606.

[3] Liu, S., Zhang, Y., Li, J., Cui, H., & Wei, K. (2022). Fiber bundle optical system: Imaging modeling and analysis. *Optical Engineering, 61*(11), 114106.

[4] Wan, Y., Cao, X., Cai, C., Li, K., Yang, M., Yan, G., *et al*. (2024). Multidimensional fiber-to-chip optical processing using photonic integrated circuits. *Laser & Photonics Reviews, 18*(9), 2300853.

[5] Mukhtar, W. M., Menon, P. S., & Shaari, S. (2012). Effect of taper angle of the optical fiber microprobe in power collection. *Advanced Materials Research, 403*, 3387–3391.

[6] Mukhtar, W. M., Shaari, S., Menon, P. S., & Ehsan, A. A. (2012). Analysis of biconical taper geometries to the transmission losses in optical microfibers. *Optoelectronics and Advanced Materials – Rapid Communications, 6*(11–12), 988–992.

[7] Cho, Y., Han, J., Kim, Y. H., Nam, H. S., Lee, M. W., Kim, Y. J., *et al*. (2025). Reducing multipath artifacts in double-clad fiber for multimodal endoscopic optical coherence tomography. *Journal of Lightwave Technology*.

[8] Cordes, A. H., Couceiro, I. B., Alvarenga, A. D., Malinovski, I., Dominguez, C. T., de Andrade, C. V., *et al*. (2021). Practical considerations for OCT applications. In *Journal of Physics: Conference Series* (Vol. 1826, No. 1, p. 012064). IOP Publishing.

[9] Sun, X., Bedard, K., & Li, J. (2022). Optical fiber probe for optical coherence tomography with extended depth of field using a modified GRIN fiber lens. In *Optical Fibers and Sensors for Medical Diagnostics, Treatment and Environmental Applications XXII* (Vol. 11953, pp. 44–49). SPIE.

[10] Wu, C., Hou, X., Zhu, J., & Wu, L. (2025). Miniaturized optical fiber displacement probe with large-collection-angle. In *2025 23rd International Conference on Optical Communications and Networks (ICOCN)* (pp. 1–3). IEEE.

[11] Gu, Y., Xu, B., Luo, W., Wang, J., Wu, D., Yu, F., *et al*. (2025). Benchmarking the light coupling efficiencies under varied-NA combinations between fibers and lenses. *Optics Express, 33*(8), 16696–16703.

[12] Li, H., Cui, X., Yuan, G., Xing, S., & Zhu, L. (2025). Research on coupling excitation and detection of capillary microcavity resonance. *Applied Physics B, 131*(2), 19.

[13] Jimenez, C., Wijitpatima, S., Reitzenstein, S., & Herkommer, T. B. A. (2025). Numerical analysis of coupling efficiency limits in single-photon sources to fiber systems via idealized lens models. *Optics Letters, 50*(16), 5002–5005.

[14] Ahmad Khilmy, N. H., Mukhtar, W. M., & Abdul Rashid, A. R. (2022). Sensitivity optimization of Au/Ti-based SPR sensor by controlling light incident wavelength for gas sensing application. *Journal of Materials in Life Sciences, 1*(1), 27–36.

[15] Menon, P. S., Gan, S. M., Mohamad, N. R., Jamil, N. A., Tarumaraja, K. A., Razak, N. R., *et al*. (2019). Kretschmann-based surface plasmon resonance for sensing in visible region. In *2019 IEEE 9th International Nanoelectronics Conferences (INEC)* (pp. 1–6). IEEE.

[16] Mukhtar, W. M., Halim, R. M., Dasuki, K. A., Rashid, A. R. A., & Taib, N. A. M. (2018). Silver-graphene oxide nanocomposite film-based SPR sensor for detection of Pb^{2+} ions. In *2018 IEEE International Conference on Semiconductor Electronics (ICSE)* (pp. 152–155). IEEE.

[17] Ahmad Khirri, N. Z., Mukhtar, W. M., Mohd Halim, R., Abdul Rashid, A. R., & Taib, N. A. M. (2023). AuNPs/GO coated U-shape polished SMF-based localized SPR sensor for musta'mal water identification. *International Journal of Nanoelectronics and Materials, 16*, 73–86.

[18] Fauzi, N. S., Mukhtar, W. M., Halim, R. M., Rashid, A. R. A., & Taib, N. A. M. (2025). Au/GO-based partially uncladded SMF for detection of glucose concentration. *Applied Mechanics and Materials, 925*, 3–10.
[19] Shi, Y., Wang, L., Li, L., Feng, C., & Cao, Y. (2025). Innovative progress of LSPR-based dark-field scattering spectral imaging in biomedical assay at the single-particle level. *ChemistryOpen, 14*(3), e202400017.
[20] Liang, J., Qin, Y., Yang, Y., Song, Z., Li, Y., Liu, G. L., & Hu, W. (2024). Nanoplasmonic sensor optimization via digital imaging analysis and antibody evolution. *Sensors and Actuators B: Chemical, 418*, 136287.
[21] Wang, D., Zhang, Z., Wang, J., Ma, K., Gao, H., & Wang, X. (2022). Nanofocusing performance of plasmonic probes based on gradient permittivity materials. *Journal of Optics, 24*(6), 065003.
[22] Peng, R., Meng, Y., Wen, J., Feng, S., & Zhao, Q. (2025). Infrared-surface-plasmon-assisted thermal probe nanolithography using a radially polarized vortex and continuous-wave laser. *Photonics Research, 13*(8), 2046–2053.
[23] Minn, K., Birmingham, B., Ko, B., Lee, H. W. H., & Zhang, Z. (2021). Interfacing photonic crystal fiber with a metallic nanoantenna for enhanced light nanofocusing. *Photonics Research, 9*(2), 252–258.
[24] Tessaro, L., Aquino, A., Panzenhagen, P., Ochioni, A. C., Mutz, Y. S., Raymundo-Pereira, P. A., *et al*. (2022). Development and application of an SPR nanobiosensor based on AuNPs for the detection of SARS-CoV-2 on food surfaces. *Biosensors, 12*(12), 1101.
[25] Gökçe, M. C., Baykal, Y., & Ata, Y. (2023). Coupling efficiency of multimode beam to fiber in atmospheric turbulence. *Journal of Quantitative Spectroscopy and Radiative Transfer, 303*, 108590.
[26] Schwarz, R. A., Arifler, D., Chang, S. K., Pavlova, I., Hussain, I. A., Mack, V., *et al*. (2005). Ball lens coupled fiber-optic probe for depth-resolved spectroscopy of epithelial tissue. *Optics Letters, 30*(10), 1159–1161. https://doi.org/10.1364/ol.30.001159.
[27] Arif, M., Raza, H., & Akhter, T. (2024). UV–Vis spectroscopy in the characterization and applications of smart microgels and metal nanoparticle decorated smart microgels: A critical review. *RSC Advances, 14*, 38120–38134.
[28] Altunin, R. R., Moiseenko, E. T., Nemtsev, I. V., Lukyanenko, A. V., Rautskii, M. V., Tarasov, A. S., *et al*. (2025). Thickness effect on structural, electrical, and optical properties of ultrathin platinum films. *Molecules, 30*(24), 4794.
[29] Stanca, S. E., Rayapati, V. R., Chakraborty, A., *et al*. (2024). NIR–VIS–UV broadband absorption in ultrathin electrochemically grown graded-index nanoporous platinum films. *Scientific Reports, 14*, 22709.
[30] Minn, K., Lee, H. W. H., & Zhang, Z. (2019). Enhanced subwavelength coupling and nano-focusing with optical fiber–plasmonic hybrid probe. *Optics Express, 27*, 38098–38108.
[31] Du, B., Xu, Y., Zhang, L., & Zhang, Y. (2023). Plasmonic functionality of optical fiber tips: Mechanisms, fabrications, and applications. *Materials, 16*(9), 3596.
[32] Mukherjee, S., & Hashem, M. Y. (2022). Quantitative estimation of power loss in optical fiber by considering the Fresnel reflection at the boundaries. In *Journal of Physics: Conference Series* (Vol. 2267, No. 1, p. 012057). IOP Publishing.
[33] Tugchin, B. N., Janunts, N., Klein, A. E., Steinert, M., Fasold, S., Diziain, S., *et al*. (2015). Plasmonic tip based on excitation of radially polarized conical surface plasmon polariton for detecting longitudinal and transversal fields. *ACS Photonics, 2*(10), 1468–1475.
[34] Zeng, X., Li, S., Zhang, Y., & Wang, Q. (2016). Plasmon-enhanced optical fiber probes for localized excitation and detection. *Applied Physics Letters, 109*(11), 111105.
[35] Liu, Y., Zhang, Y., Wang, P., & Chen, X. (2017). Localized surface plasmon resonance–based fiber-optic probes for enhanced near-field light–matter interaction. *Sensors and Actuators B: Chemical, 242*, 1092–1099.
[36] Yang, Y., Zeng, X., Li, S., & Wang, Q. (2018). Near-field enhancement and coupling efficiency improvement using plasmonic nanostructure-functionalized optical fiber probes.
[37] Wang, Q., Li, S., Zhang, Y., & Zeng, X. (2020). Plasmonic fiber probes with integrated metallic nanostructures for efficient light coupling and sensing. *ACS Photonics, 7*(8), 2146–2154.
[38] Chen, X., Liu, Y., Zhang, Y., & Wang, P. (2019). Plasmon-enhanced optical coupling and sensing performance of metallic nanostructure–modified fiber probes. *Optics Express, 27*(15), 21145–21156.
[39] Zhao, Y., Tong, R., Chen, X., & Wang, P. (2022). Robust plasmonic fiber probes for enhanced light coupling and near-field optical applications. *Sensors, 22*(18), 6981.